JOURNAL OF CATALYSIS 109, 12–24 (1988)

An Integrated Study of $Pt/WO_3/SiO_2$ Catalysts for the NO–CO Reaction

III. FTIR Kinetic Study and Correlation of Promotional Effects

J. R. REGALBUTO[1] AND E. E. WOLF[2]

Department of Chemical Engineering, University of Notre Dame, Notre Dame, Indiana 46556

Received March 31, 1987; revised August 17, 1987

The kinetics of the NO–CO reaction and promotion mechanism of WO_3 on $Pt/WO_3–SiO_2$ catalysts was studied by FTIR spectroscopy in an *in situ* recycle IR microreactor. It was found that addition of WO_3 to Pt/SiO_2 increased activity toward the NO–CO reaction. The kinetics displayed an inhibition behavior with increasing CO concentration, but WO_3 served to decrease CO surface coverage during the inhibited regime. However, the rate of NO dissociation over Pt was slowest for the most active (tungsta-containing) catalysts. Characterization studies showed previously that addition of WO_3 resulted in the decoration of Pt crystallites by suboxides of WO_3. The promotional effects and kinetic results are explained in terms of the participation of $Pt–WO_x$ adlineation sites, which resulted from the decoration effect. Using this concept, a correlation between the increased activity and the concentration of adlineation sites successfully explained the kinetics and IR results obtained with all the catalysts used. The addition of WO_3 to Pt/SiO_2 is believed to produce a small number of adlineation sites having very high NO dissociation activity.

INTRODUCTION

In parts I and II of this study, an SMSI morphology has been demonstrated for $Pt/WO_3/SiO_2$ catalysts through characterization by XRD, chemisorption and XPS (*1*), and TEM (*2*). The suppression of CO chemisorption on Pt was postulated to arise from decorating patches of partially reduced "WO_x" (likely WO_2) species. The impact of this promoted catalyst's morphology on the NO–CO reaction might be envisioned by considering Fig. 1. It was postulated (*1*) that WO_3 might serve to increase the rate of NO dissociation, the rate-determining step of the NO–CO reaction at reducing stoichiometries, if active tungsten sites in close proximity to Pt sites could be produced. As seen in the figure, Pt sites adjacent to decorating overlayers of WO_x may correspond to such sites. Because they appear at the one-dimensional boundary between two solid phases, these sites have been termed "adlineation" sites (*3*). These types of sites have lately been implicated in higher $CO–H_2$ synthesis activity over Pt/TiO_2 and Pd/La_2O_3 catalysts (*4*), as well as in higher NO dissociation activity over Rh/TiO_2 (*5*, *6*). Although an SMSI morphology was not invoked, $Pt^0–Mo^{4+}$ complexes were postulated to display activity similar to Rh for NO reduction by CO (*7*).

SMSI enhancement of catalytic activity has also been suggested to be largely electronic in nature. Overlayers containing Mo^{2+} and Mo^{4+} were postulated to stabilize rhodium ions and so to increase synthesis gas conversions (*8*). Interaction between Rh and Ti^{3+} ions has been suggested to account for improved NO reduction by CO (*9*).

To determine the impact of $Pt–WO_x$ sites on the NO–CO reaction, catalyst activity and the behavior of adsorbates of NO and

[1] Present address: Dept. of Chemical Engineering (m/c 110), University of Illinois at Chicago, Box 4348, Chicago, IL 60680.

[2] To whom correspondence should be addressed.

0021-9517/88 $3.00

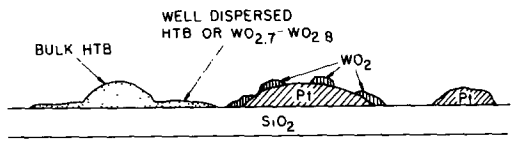

FIG. 1. Schematic representation of the morphological configuration of the Pt/WO_3–SiO_2-supported catalysts.

CO were monitored simultaneously and *in situ* by fitting a recycle loop to a FTIR microreactor. A similar setup has been used by this group in the study of CO and ethylene oxidation (*10, 11*). The purposes of the recycle stream are to increase the rate of heat transfer from the catalyst into the gas phase and to increase mixing within the reactor. Without the recycle, because of the exothermicity of the reaction and low flow rates, significant differences between the catalyst surface temperature and the gas phase occur (*10, 12*), which prevent true kinetic observations.

Kinetic and mechanistic results from the low- and high-tungsta catalysts were compared qualitatively to those from the tungsta-free series. Additionally, the effects of the promoter were correlated quantitatively to those of previously characterized catalysts (*1, 2*). With measurements from XPS and selective chemisorption, a novel correlation was obtained between CO_2 production and numbers of active sites. This correlation also served to indicate which mechanistic step was most influenced by the presence of the promoter. As the final step in the integration of kinetic, mechanistic, and characterization data, the NO–CO reaction has been numerically simulated by an elementary step reaction model (*12*).

EXPERIMENTAL

FTIR Spectrometer and Microreactor

A Digilab FTS 15C FTIR equipped with a liquid-nitrogen-cooled mercury–cadmium telluride detector and a high-intensity ceramic source was employed. The spectrometer–microreactor system has been described in detail previously (*10, 12*); however the microreactor used for the present work was fabricated from aluminum, not stainless steel, to minimize the catalytic activity of the reactor itself. The reactor was operated mostly in a recycle mode, using a double-diaphragm, Teflon-lined reciprocating pump (Mosier Fluids, Model 2107). Tubing for the recycle loop was connected to the reactor inlet and outlet about 6 cm away from the reactor flanges. For a nominal flow rate of 200 cm^3/min and a recycle ratio of approximately 50 : 1, the effective reactor volume was 160 cm^3 and the reactor was isothermal to within 5°C. Also, reactor pressure was raised 5 to 10 psig above atmospheric. A section of aluminum tubing was used as a preheater, again to avoid the activity of stainless steel toward the NO–CO reaction. Control runs at a reactor temperature of 280°C showed no significant conversion.

FTIR experiments included CO concentration-programmed reaction (CPR) with NO at 220 and 280°C and NO dissociation at 220 and 280°C. CPR experiments were carried out by linearly increasing and then symmetrically decreasing the mass flow of CO between zero and 1.27 or zero and 29 cm^3/min. At a carrier gas flow rate of 180 cm^3/min these corresponded to concentration "ramps" of approximately 0–0.7–0% and 0–14–0%, respectively.

At 280°C, considerable NO dissociation occurred. In order to begin high-temperature (280°C) CO CPR at full NO surface coverage, a small amount of CO was pulsed into the NO-containing feed. With CO on the Pt surface, any oxygen that accumulated from NO dissociation was reacted away. The start of the experiment was timed for the point when CO–Pt coverage returned to zero, and NO–Pt coverage was nearly full. A similar procedure was used to obtain full NO surface coverage at the start of an NO dissociation experiment.

During the CPR experiments, infrared data were collected in sets of 500 spectra

over approximately 2 h. Each spectrum consisted of 60 accumulated scans at 8-wavenumber resolution. CO and CO_2 effluent concentrations were monitored by Beckman Models 315 and 865 IR analyzers. Reactor gas phase and "surface" temperature were monitored as well.

Materials

Catalyst compositions are listed in Table 1, and their preparations are given in Part I of this work (*1*). The same nomenclature is used here to identify metal loadings: tungsta-free (Pt/SiO_2), low-tungsta ($Pt/WO_3/SiO_2$), and high-tungsta (Pt/WO_3–SiO_2). Catalyst wafers 2.5 cm in diameter were pressed from approximately 45 mg of the reduced catalysts at 7000 lb/in^2. Wafers were trimmed to approximately 2 cm in diameter after they were mounted in the holder. Catalysts were weighed directly upon removal from the reactor, after reaction studies had been completed.

After being placed in the reactor, wafers were reduced *in situ* in H_2 for 3 h at 200°C. Prior to high-temperature (280°C) reaction studies, catalysts were aged in a 2% CO, 1% NO feed until the height of the CO–Pt peak remained constant. This was usually done by an overnight treatment at 220°C.

Ultrahigh-purity H_2 and N_2 were used along with CP-grade O_2 and research-grade CO (Linde). CO was purified further for iron carbonyls by a molecular sieve trap cooled in a dry ice–acetone mixture. CP-grade NO (Matheson) containing N_2O (200 ppm) and N_2 (0.54%) impurities was used. N_2O was also eliminated by a cooled molecular sieve trap.

RESULTS

CO Concentration-Programmed Reaction

CO concentration was programmed 0–14–0% into a 10% NO feed at 220°C over a number of the low- and high-tungsta catalysts. Behavior of adsorbates of CO and NO were similar for both loadings. At this lower temperature, CO_2 was never produced in more than trace amounts. A representative series of spectra illustrating the CO CPR experiment over the tungsta-containing catalysts is shown in Fig. 2a and compared to the identical experiment performed over a tungsta-free catalyst (Fig. 2b, (*13*)). Gas-phase bands for CO and NO are centered at 2143 and 1870 cm^{-1}, respectively. In both experiments, CO–Pt adsorbates quickly displaced NO–Pt species and dominated the Pt surface over most of the experiment. Two small yet distinct differences were observed in the spectra of Fig. 2a, one being a 1400-cm^{-1} band which was present in small quantities for most of the experiment. The other was a left-hand shoulder at roughly 2100 cm^{-1} on the

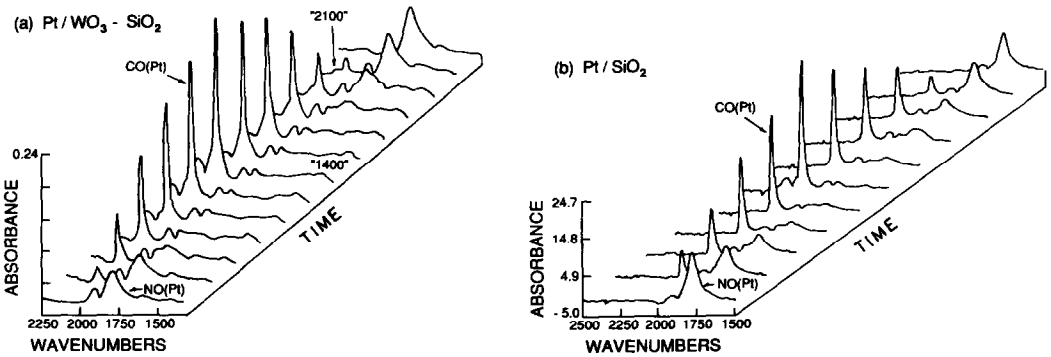

FIG. 2. IR spectra during a CO CPR (0–14–0% CO) into 10% NO at 220°C, at various time intervals showing the species present. (a) Pt/WO_3–SiO_2 catalyst; (b) Pt/SiO_2 catalyst.

CO–Pt band. By comparing equivalent peak heights of the CO–Pt species at the beginning and end of the figure, one can see that the 2100-cm^{-1} species slowly accumulated over the course of the experiment. Low-tungsta catalysts used in this experiment also exhibited these 2100- and 1400-cm^{-1} infrared bands, in slightly lower intensities than for the high-tungsta catalysts. No bands other than those shown in the spectrum were observed; consequently regions containing no bands were excluded from the figures.

A comparison of the spectrograms of all species in these two experiments is made in Figs. 3a (5Pt/WO_3/SiO_2 catalyst) and 3b (5Pt/SiO_2 catalyst). The spectrograms of CO–Pt and NO–Pt in Figs. 3, 4, and 6 were scaled by their maximum absorbance and therefore approximate surface coverage under the assumption that the extinction coefficients are constant. The behavior of these two adsorbates is roughly the same. NO–Pt peak heights on both catalysts were higher at the end of the experiments than at the beginning, indicating that initially NO may have been dissociated to a small extent.

A spectrogram of the 2100-cm^{-1} species was produced by choosing a frequency window far enough from the linear CO–Pt peak that changes in CO–Pt coverage would not affect it, and then subtracting the effect of gas phase CO from this spectrogram. This and a spectrogram of the 1400-cm^{-1} species are also plotted in Fig. 3a. To keep their relatively small intensities in perspective, these spectrograms were divided by the maximum CO–Pt peak height. The 2100-cm^{-1} species slowly accumulated until linear CO–Pt species had almost completely left the surface. The accumulation of the 1400-cm^{-1} species was rapid at the beginning of the experiment but did not change much thereafter.

It should be mentioned that neither of these two new bands, at 2100 and 1400 cm^{-1}, was observed when only one reactant, either CO or NO, was present. They were only observed when NO and CO were present simultaneously. Also, no IR bands were observed when NO and/or CO were passed over a Pt-free, reduced 6.2 WO_3/SiO_2 catalyst at temperatures up to 260°C.

The production of CO_2 became appreciable at a temperature of 280°C, as CO concentration was ramped 0–0.7–0% into a 2% NO feed. The CO feed concentration and CO_2 production from representative catalysts of the WO_3-free, low-tungsta, and high-tungsta series are shown in Fig. 4a. Corresponding spectrograms of linear CO–Pt are shown in Figure 4b, NO–Pt spectrograms in Fig. 4c, and representative spectrograms of the 2100- and 1400-cm^{-1} bands in Fig. 4d.

Two regimes of CO_2 production were observed. Initially, CO conversion was high and of positive order in CO feed concentration (Fig. 4a). Later, conversion became low and of negative order in CO concentration. The transition between the

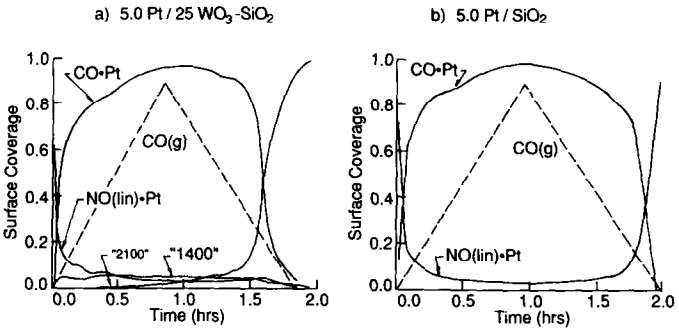

FIG. 3. Spectrograms of CO–CPR studies shown in Fig. 2. (a) Pt/WO_3–SiO_2; (b) Pt/SiO_2.

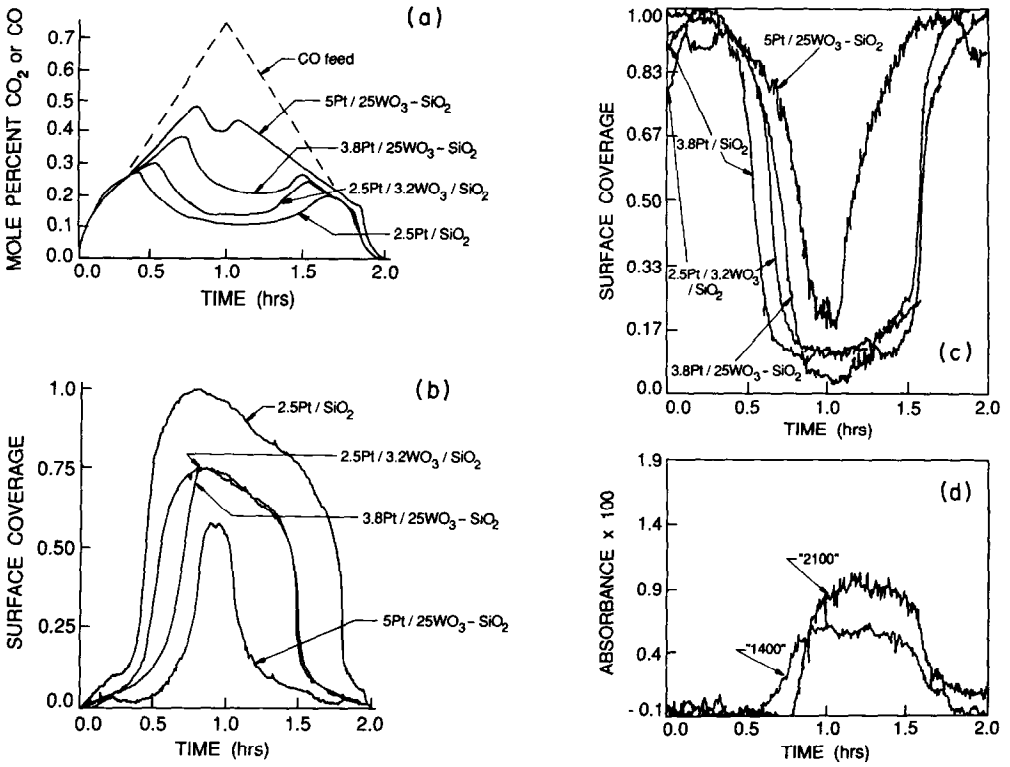

FIG. 4. CO–CPR (0–0.7–0% CO) into 2% NO at 280°C over representative promoted and unpromoted catalysts. (a) CO_2 production and CO concentration versus time; (b) CO–Pt spectrograms; (c) NO–Pt spectrograms; (d) representative spectrograms of the 2100 and 1400 cm^{-1} bands.

two regimes was marked in every case by a rapid increase in CO–Pt coverage (Fig. 4b). For the most part, NO–Pt coverage (Fig. 4c) was inversely proportional to CO–Pt coverage, being displaced by CO–Pt at the transition between regimes. At the beginning of the experiments, slight deviations from this proportionality were observed. NO–Pt coverage of the least active catalysts was below full coverage and increased as the reaction began, whereas NO–Pt coverage for the most active catalysts was always nearly full. The 2100- and 1400-cm^{-1} species (Fig. 4d) were not observed under the high-conversion regimes, but did accumulate as CO–Pt accumulated.

The beneficial promotional effect of WO_3 is clear in Fig. 4. Two trends were noted with increased catalytic activity. First, more CO_2 was produced as the reaction proceeded farther into the concentration ramp before the transition to high CO–Pt coverage (CO inhibition) occurred. Second, when the CO–Pt coverage did increase, it did not appear to increase as much for the more active catalysts. In general, it appeared that tungsta serves to remove some degree of CO inhibition.

To compare the activity of all catalysts quantitatively, the CO_2 production rate at the center of the experiments (at maximum CO concentration) was used. This particular point was chosen as most representative of steady-state behavior. A summary of CO_2 production rates (molecules/sec, molecules CO_2/sec/g Pt) for all catalysts tested is given in Table 1.

NO Dissociation

NO dissociation was detected by monitoring the height of the NO–Pt band as a function of time under relatively nonreac-

TABLE 1

CO_2 Production over Unpromoted and Promoted Catalysts

Catalyst	Catalyst loading (g)	r_{CO_2} (10^{17} molecules/sec)	r_{CO_2}/wt Pt (10^{18} molecules/sec/g Pt)
2.5Pt	0.0293	0.747	2.55
3.8Pt	0.0375	1.25	3.33
5.0Pt	0.0346	1.33	3.84
$1.2Pt/4.7WO_3$	0.0548	0.789	1.44
$2.5Pt/3.2WO_3$	0.0402	0.913	2.27
$3.8Pt/1.7WO_3$	0.0491	0.664	1.31
$1.2Pt/25WO_3$	0.0371	0.789	2.13
$3.8Pt/25WO_3$	0.0362	1.83	5.06
$5.0Pt/25WO_3$	0.0361	2.82	7.81

tive conditions at 220°C and during reactive conditions at 280°C.

NO dissociation experiments were first performed at 220°C on the $5Pt/SiO_2$ and $5Pt/25WO_3$–SiO_2 catalysts. Short pulses of CO introduced into a 5% NO stream had the effect of removing any adsorbed oxygen produced from prior NO dissociation. Behavior of the NO–Pt and CO–Pt species was similar over both catalysts; NO–Pt and CO–Pt spectrograms from the $5Pt/25WO_3$–SiO_2 catalysts are shown in Fig. 5a. After a CO pulse, CO–Pt abruptly removed almost all the NO–Pt, which then reaccumulated to a peak height 30% above the previous steady-state height (20% for the $5Pt/SiO_2$ catalyst), but within 3 min returned to almost the same level. In the next 40 min the NO–Pt peak height decreased by only a few percent, confirming that almost no NO dissociation was occurring. In both experiments, only minute quantities of CO_2 were produced in the first few minutes following a pulse.

The 1400–1500-cm^{-1} bands for the unpromoted and promoted catalysts are shown in Figs. 5b and 5c. One major difference was observed between the spectra from the $5Pt/SiO_2$ catalyst (Fig. 5b) and the $5Pt/25WO_3$–SiO_2 catalysts (Fig. 5c). This was again the small peak located at wavenumber 1420 over the $5Pt/25WO_3$–SiO_2 catalyst. Its spectrogram is plotted in Fig. 5a; it appeared just after the CO pulse and its disappearance lagged slightly behind that of the CO–Pt peak. The 2100-cm^{-1} band was not observed in this experiment; apparently CO did not contact the Pt surface long enough for this species to accumulate in measurable quantities.

NO dissociation experiments at 280°C were performed for all three catalyst series, directly after the 280°C CO CPR experiments. As is shown for representative catalysts in Fig. 6, NO dissociation led to substantial decreases in the NO–Pt peak heights (normalized in this figure to approximate surface coverage). The decrease in NO–Pt surface coverage is due to the increase in the coverage of strongly adsorbed oxygen species (O–Pt) resulting from NO dissociation. O–Pt species do not desorb at this temperature and thus occupy sites that are no longer available for NO adsorbates. The interesting result revealed in Fig. 6 is that the catalysts having the highest NO–CO activity (Fig. 4a, $3.8Pt/25WO_3$–SiO_2 and $5Pt/25WO_3$–SiO_2) actually exhibited the slowest NO dissociation on Pt. That is, the rate of NO dissociation on Pt decreased with increasing WO_3 loading.

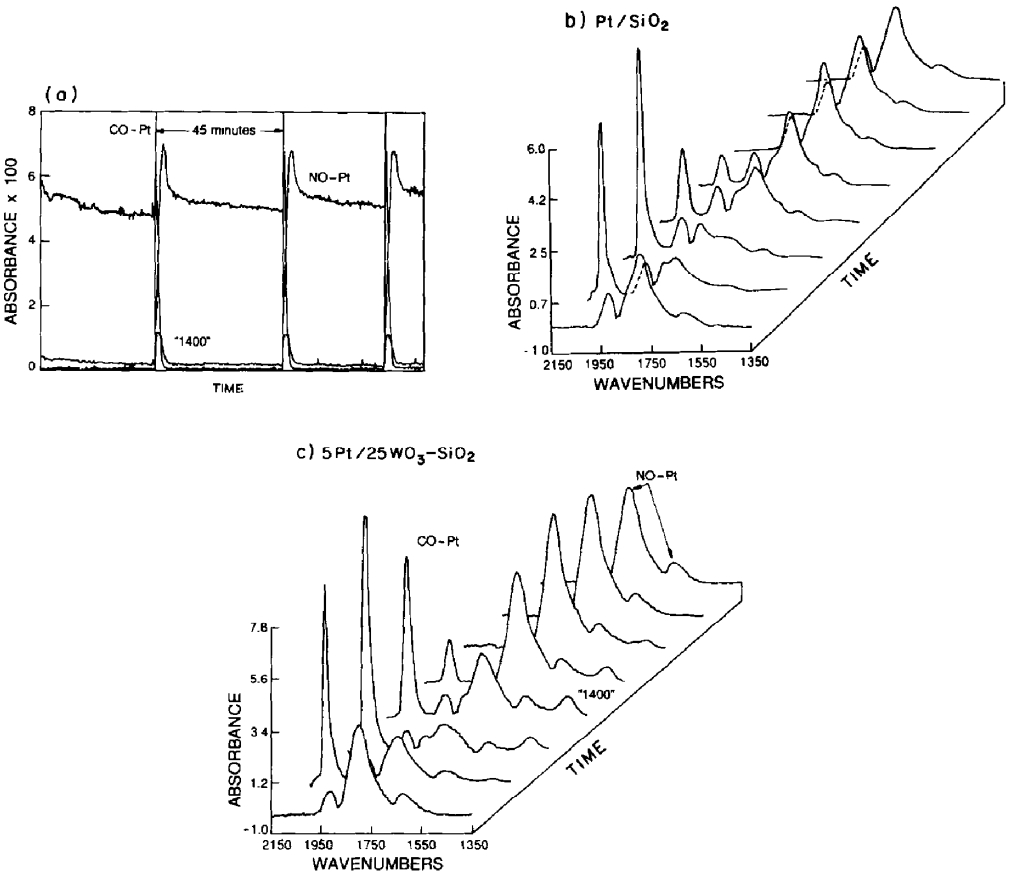

FIG. 5. CO pulsing into 5% NO at 220°C. (a) Spectrograms for CO–Pt, NO–Pt, and the 1400-cm^{-1} band; (b) time-dimension spectra for the $5Pt/SiO_2$ during a CO pulse; (c) same as (b) but on the $5Pt/25WO_3–SiO_2$ catalyst and clearly showing the 1400-cm^{-1} species.

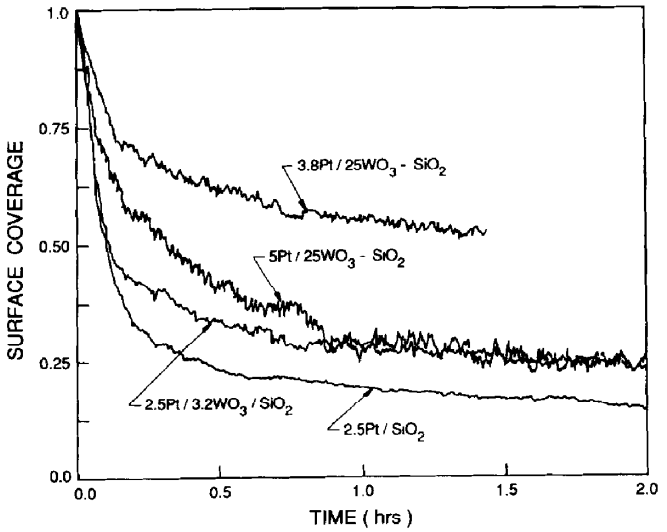

FIG. 6. Normalized absorbance or surface coverage of the NO–Pt spectrograms over promoted and unpromoted catalysts during dissociation experiments at 280°C and 2% NO.

Effect of WO_3 on Characteristic Absorbance of Pt

In an effort to examine any electronic effect on CO–Pt bonding strength, the characteristic absorbance of the linear CO–Pt species was recorded for all catalyst series at 220 and 280°C. Results are given in Table 2, along with Pt $4f_{7/2}$ electron binding energies for the same catalysts (*1*). At 220°C, small shifts in characteristic absorbance correlated well to electron binding energy. The catalysts with the highest ebe, 71.2 eV, absorbed CO at 2083 cm^{-1}, while an 8-wavenumber increase to 2091 cm^{-1} was observed for the two catalysts that had electron binding energies of 70.5 eV. At 280°C, characteristic absorbance did not correlate well with Pt $4f_{7/2}$ ebe, but shifted upscale with increased tungsta loading. For the high-tungsta series, characteristic absorbances were 8–10 cm^{-1} higher than the range of 2069–2072 cm^{-1} exhibited by the tungsta-free series.

DISCUSSION

The major findings of the FTIR and kinetic study of the NO–CO reaction over $Pt/WO_3/SiO_2$ catalysts can be summarized as follows:

1. During CO CPR experiments at 220°C over low- and high-tungsta loaded catalysts, no appreciable CO_2 was produced. Behavior of CO–Pt and NO–Pt species was very similar to that observed over the unpromoted catalysts. Two new peaks of low relative intensity were observed over the tungsta-containing catalysts, one at 1420 cm^{-1} and another at 2100 cm^{-1}.

2. During reactive CO CPR experiments at 280°C, two reaction regimes were observed, one of high CO conversion and positive order in CO (gas) concentration; the other of low conversion and negative order in CO. Transition between the two regimes was accompanied by a rapid increase in CO–Pt coverage. NO–Pt coverage was inversely proportional to CO–Pt coverage, except for small regions at the beginning of some experiments. The 2100- and 1400-cm^{-1} bands accumulated only after the transition to the CO-inhibited regime had occurred.

3. In NO dissociation experiments at 220°C, the absorbance of NO–Pt species following a CO pulse was similar over a tungsta-free and a high-tungsta catalyst; after an initial decrease of between 20 and 30%, the NO–Pt peak height was almost constant for long periods of time. The 1400-cm^{-1} species appeared over the high-tungsta catalyst but the 2100-cm^{-1} species did not.

4. Through NO dissociation experiments conducted at 280°C it was determined that the catalysts that were the most active toward the NO–CO reaction (at 280°C) exhibited the least activity toward NO dissociation on Pt.

TABLE 2

Variation of CO–Pt Absorbance with Pt $4f$ ebe

Catalyst	Pt $4f_{7/2}$ ebe	Wavenumber (cm^{-1})	
		220°C	280°C
2.5Pt	71.2	—	2069
3.8Pt	71.1	—	2069
5.0Pt	70.9	2087	2072
$1.2Pt/4.7WO_3$	71.2	2083	2073
$2.5Pt/3.2WO_3$	70.5	2091	2073
$3.8Pt/1.7WO_3$	70.7	2087	2070
$1.2Pt/25WO_3$	70.9	2087	2077
$2.5Pt/25WO_3$	70.7	2087	2077
$3.8Pt/25WO_3$	70.5	2091	2079
$5.0Pt/25WO_3$	70.9	2087	2081

Previous extensive characterization results (*1*, *2*) have led to the model of the surface depicted in Fig. 1. The working hypothesis of this study is that the activity and FTIR results must correlate with the characterization measurements to validate the morphologic model.

The first step in establishing a correlation is the identification of the observed IR bands. The CO–Pt band (2079 cm^{-1}, linear CO) and NO–Pt bands (1795 and 1620 cm^{-1}, linear and bridged or bent NO) are well known, consequently the identification

of the 2100-cm^{-1} and 1400-cm^{-1} bands remain. The proximity of the 2100-cm^{-1} band to CO–Pt suggests that it is an adsorbed form of CO. No information is available on the IR adsorbance of CO on WO_3 nor was CO detected on the Pt-free tungsta catalysts. However, CO adsorbed on polycrystalline W at room temperature and ultrahigh vacuum was reported to exhibit a band in the 2093–2117-cm^{-1} range (*14*). The characterization work indicated that no elemental tungsten existed in the $Pt/WO_3/SiO_2$ catalysts (*1*), but was present in the form of hydrogen–tungsten bronzes (HTB) or tungsten suboxides (WO_x). It follows that the 2100-cm^{-1} band can be attributed to CO adsorbed on these decorating WO_x suboxides or at its interface with Pt (adlineation sites).

The 1400-cm^{-1} species seen in Figs. 2, 4, and 5c is likely an oxidized NO analog of the CO–WO_x species. Nitrate ($-NO_2$ or $-NO_3$) forms of nitrogen oxide have been reported on Rh at 1550, 1295, and 1240 cm^{-1}, shifted as much as 870 cm^{-1} from other molecular NO adsorbates (*15*). A nitrate form has also been reported to adsorb on TiO_2 in Pt/TiO_2 catalysts (*16*) at 1473 cm^{-1} and on reduced "TiO_x" sites in Rh/TiO_2 catalysts (*5, 6*) between 1500 and 1400 cm^{-1}. It appears that the characteristic absorbance of the nitrate is relatively independent of the substrate.

The 1400-cm^{-1} band is not the isocyanate band since no band was observed at 2350 cm^{-1} that could be attributed to the asymmetric isocyanate stretch. The behavior of these species during the nonreactive (220°C) CO CPR experiment is notable. CO–WO_x (2100 cm^{-1}) accumulated only after significant amounts of CO–Pt formed. Additionally, no CO–WO_x species were observed unless NO was also present as a reactant. The accumulation of CO on Pt–WO_x sites is therefore analogous to hydrogen spillover, but CO spillover seems to be NO-assisted. NO spillover, or the formation of NO_x–WO_x, occurs much faster than CO spillover, but similarly requires the assistance of CO. The 2100- and 1400-cm^{-1} species appeared on both the low- and high-tungsta catalyst series. This implies that even though they were not detected by XPS (*1*), small amounts of WO_3 were reduced beyond HTBs to WO_x in the low-tungsta catalysts.

Once the observed IR bands have been assigned, there remains the ascertainment of which mechanistic steps are beneficially affected by tungsta to produce the higher activity.

The CO–Pt and NO–Pt spectrograms over the promoted and unpromoted catalysts are very similar (Fig. 3). From this observation one can conclude that the ratio of NO and CO coverages are similar in both catalyst series. If one assumes that the rates of adsorption of NO and CO are the same, it follows from elementary step kinetics (*17*) that under equilibrium conditions and for the same ratio of gas phase concentrations, the ratio of desorption rates (CO to NO) must be the same in both catalytic series (*12, 17*). Furthermore, the relatively small shift in CO–Pt absorbance for tungsta-containing catalysts indicates that the absolute rate of CO desorption is not significantly altered. Shifts of 20 cm^{-1} were also considered inconsequential for CO adsorption on Pd/La_2O_3 (*18*). It was only when shifts of 50 cm^{-1} were detected with Rh/TiO_2 catalysts (*9*) that inference was made to an electronic SMSI effect. It appears that increased activity is not due to an increase in the desorption rate of CO over the promoted catalysts.

The next step that must be analyzed is the rate of NO dissociation. NO dissociation is evidenced in the dissociation experiments (Fig. 5) by decreases in NO surface coverage. This is caused by the accumulation of atomically adsorbed oxygen, which does not desorb at these temperatures. This agrees with Pt single-crystal studies, which have demonstrated that only one low-index Pt plane, the (110), is active toward NO dissociation (*19*). The behavior at 220°C (Fig. 5) indicates that

only 20 to 30% of the Pt surface is active toward NO dissociation. At 220°C there does not appear to be a great difference between the Pt dissociation activity of the unpromoted and promoted catalysts; the majority of the Pt surface in each appears to be inactive toward NO dissociation.

At 280°C, however, there is a steady rapid decline of the NO–Pt peak on the unpromoted catalysts (Fig. 6), indicating that NO dissociation is occurring over an appreciable fraction of the surface. This in turn may signify that surface defects in previously inactive facets become active or that surface diffusion to active sites becomes important at the higher (280°C) temperature. The overall result of the 280°C dissociation experiment is that the decrease in NO coverage with time over Pt is lower on the promoted catalysts than on the unpromoted ones. The rate of NO dissociation depends on N_{Pt}, and this number is greater for the most active catalysts, i.e., $5Pt/25WO_3–SiO_2$, (see Table 3). Consequently the coverage decrease for the promoted catalysts, which is normalized by N_{Pt}, has the highest slope. It has been suggested that SMSI catalyst supports such as TiO_2 might serve to create higher-order Pt planes of high dissociation activity (*23*). Such is not the case for WO_3, however. The lower dissociation rates in the promoted catalyst might also be due to the reduction in the numbers of adjacent open sites required for NO dissociation, caused by the decorating patches of WO_x or by their hindrance of surface diffusion. The increased activity in the promoted catalysts is not a consequence of increased NO dissociation over Pt. However, dissociation products must have their source somewhere and since bulk tungsta itself is not active nor does it adsorb NO or CO, the only other source for increase in NO–CO reaction rates is via sites at the interface of the decorating WO_x patches on Pt crystallites. These sites, referred to in the literature as adlineation sites, have been previously proposed to explain qualitatively the increased activity in SMSI catalysts (*4–6*). The small IR bands at 2100 and 1400 cm^{-1} can be adscribed to CO and NO adsorbed on these adlineation sites.

TABLE 3

Calculated Values of N_{Pt} and N_{PtW}

Catalyst	N_{Pt} ($\times 10^{17}$)	N_{PtW} ($\times 10^{14}$)	N_{PtW}/N_{Pt} ($\times 10^{-3}$)
2.5Pt	3.87	—	0
3.8Pt	5.47	—	0
5.0Pt	4.00	—	0
$1.2Pt/4.7WO_3$	1.96	3.72	1.90
$2.5Pt/3.2WO_3$	2.43	3.65	1.50
$3.8Pt/1.7WO_3$	3.65	2.92	0.80
$1.2Pt/25WO_3$	0.364	12.8	35.2
$2.5Pt/25WO_3$	0.788	18.6	23.6
$3.8Pt/25WO_3$	1.22	22.3	18.3
$5.0Pt/25WO_3$	1.90	27.9	14.2

It is noted, however, that the $CO–WO_x$ and $NO–WO_x$ species do not appear to be reaction intermediates since they appear only under nonreactive conditions when CO has inhibited the dissociation of NO. In the complete absence of CO, the adlineation sites should also be inactive since there is no mechanism for their regeneration via oxygen removal by the coreactant.

While the concept of adlineation sites is not new, a quantitative correlation between increased activity and the concentration of these sites has not been reported. The extensive catalyst characterization conducted previously (*1*) permits an attempt at such a correlation for the first time. This correlation is based on the assumption that the observed activity is the result of the contributions of the Pt sites and of the adlineation sites. A successful correlation should relate the observed rates with the concentration of each type of site as determined from the characterization results.

From the CO_2 production rates and Pt loadings given in Table 1 and the number of surface sites in each catalyst (N_{Pt}) determined from CO chemisorption (*1*), an

average turnover number TON_{Pt} = 0.25 molecules/Pt site/sec was calculated for the unpromoted Pt/SiO_2 catalysts. The maximum rate of CO_2 production obtained from the CO-CPR spectrograms (Fig. 4 and Table 1), divided by the product $N_{Pt} \times TON_{Pt}$, i.e., by the contribution of Pt sites only, is shown in Fig. 7a. If Pt sites were the only contribution to the observed activity, the above ratio should be equal to unity, as is the case for the unpromoted catalysts and to a less satisfactory degree for the low-tungsta catalysts. However, there is a large discrepancy for the high-tungsta loading catalysts, which yields a ratio several times larger than one.

The contribution of the adlineation sites can be written in form analogous to that of the Pt sites, i.e., equal to the product of their turnover number TON_{PtW} times their surface concentration N_{PtW}. If the total rate is assumed to be the sum of the contribution of each site, then

$$r_{CO_2} = TON_{Pt}N_{Pt} + TON_{PtW}N_{PtW}. \quad (1)$$

While in a supported catalyst is not possible to calculate the number of adlineation sites N_{PtW} unequivocally, an estimate can be made on the basis of surface concentration measurements of both components in the catalysts. Figure 7b shows the W surface atomic percent measured by XPS versus the weight percent Pt; these data exhibit a trend similar to that of Fig. 7a. This suggests that the concentration of adlineation sites is related to the surface concentration of W measured by XPS, N_{Ws}. If the distribution of Pt and WO_x is random, the probability of one being deposited onto the other (thus generating adlineation sites), is proportional to the product of their surface concentrations. Thus, as a first approximation, it can be assumed that $N_{PtW} = N_{Ws}N_{Pt}$, where N_{Pt} is measured from CO chemisorption. It should be noted that the Pt signal from XPS cannot be used for this calculation. Very thin decorating layers of WO_x would block Pt chemisorption sites but would not block all of the XPS Pt signal from underlying Pt; since the XPS signal arises from a depth of about 20 Å. XPS figures for N_{Pt} are artificially high. The most accurate measurement of N_{Pt} is then the CO chemisorption measurement. A further note is that this type of calculation could not be extended to systems in which chemisorption is nonselective.

Values of N_{Pt} and N_{PtW} for each catalyst calculated from chemisorption data and the W XPS signal are listed in Table 3. For all catalysts, N_{PtW} is at least 30 times smaller

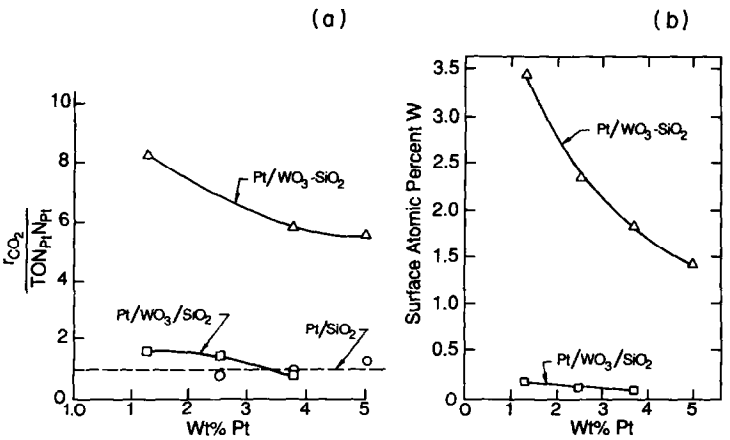

FIG. 7. (a) CO_2 production rates normalized over the production rate due to Pt sites only versus Pt loading; (b) XPS W surface atomic % versus Pt loading.

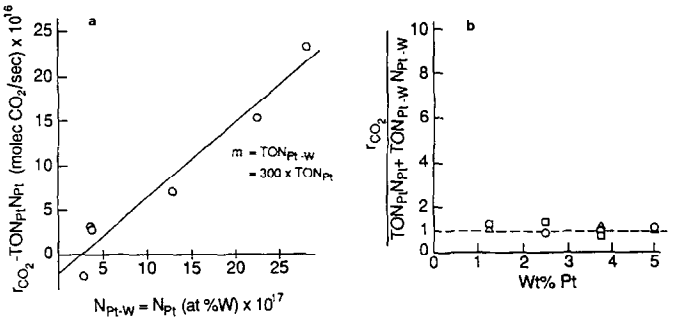

FIG. 8. CO_2 production difference due to Pt–W sites only versus the product of W–XPS surface atomic % and N_{Pt} or N_{PtW}; (b) CO_2 production rate normalized by the separate contribution of the Pt and PtW sites.

than N_{Pt}. It is noted that these figures are in line with the relative intensities of the CO–WO_x or NO–WO_x IR bands.

To test this calculation for N_{PtW}, the difference $r_{CO_2} - TON_{Pt}N_{Pt}$ for the promoted catalysts, which represents the contribution of only the adlineation sites to CO_2 production, is plotted in Fig. 8a versus the product $N_{W_S}N_{Pt}$. N_{Pt} again is the chemisorption value, and TON_{Pt} is known from the unpromoted catalysts. Figure 8a shows that the data thus plotted roughly fit a straight line with a slope equal to $TON_{PtW} = 92$ molecules/PtW site/sec, which is about 360 times greater than TON_{Pt}. The negative value near the origin in the plot arises as a result of the low activity of this catalyst (3.8 Pt/1.7WO_3/SiO_2), introducing inaccuracy in the measurement of its reaction rates.

An alternative representation of the correlation is shown in Fig. 8b, where the left hand side of eq. (1) divided by the right hand side is plotted versus wt% Pt. It can be seen that the data for all the catalysts studied, unpromoted and promoted high- and low-tungsta, fall on a single line equal to unity, in contrast to the first correlation based on Pt sites only (Fig. 7a).

The correlation suggests that a small number of very active sites are responsible for the observed promotional effects (see Table 3). The turnover number of the adlineation sites, TON_{PtW}, can be taken as only an order of magnitude estimate since the concentration of the adlineation sites N_{PtW} is only the best estimate that can be made with these complex catalysts. More accurate estimates of the concentration of adlineation sites requires the use of model catalysts such as those used by Bell *et al.* (*24*) and Gorte *et al.* (*25*). Nonetheless, the fact that a quantitative correlation among various catalysts has been attained by separate measurements of activity and surface composition is indeed remarkable and supports in general a dual-site mechanism. Kinetic work using an elementary step model (*12*), similar to the one employed for CO oxidation (*22*), has shown that the FTIR results shown in Figs. 2–6 can be simulated only when a mechanism involving Pt and Pt–WO_x sites is assumed.

While a qualitatively and quantitatively consistent pathway for the promotional effects observed has been presented, the specific nature of the adlineation sites and why they exhibit higher activity can not be determined. The low concentration of such sites prevents the contribution of their surface signals from being differentiated from the signals of Pt, WO_3, and CO and NO adsorbed on Pt. Thus changes in the Pt 4*f* electron binding energies and shifts in characteristic IR frequencies, which were small in the first place, can not be uniquely associated with the adlineation sites. Kinetic modeling results have shown that a reaction pathway that is consistent with both the

activity and NO dissociation results is a redox cycle for saturating and regenerating the decorating the WO_x–Pt adlineation sites. This reaction pathway is also consistent with the two-site correlation, the 2100- and 1400-cm^{-1} IR bands, the XRD and XPS measurements supporting the existence of surface suboxides, and the TEM data on model catalysts showing the formation of overlayers at the interface of Pt and WO_x crystallites.

In summary, a comprehensive study of the NO–CO reaction on $Pt/WO_3/SiO_2$ catalysts, combining surface analysis, IR spectroscopy, TEM, and kinetics modeling, has led to a consistent understanding of the promotional effects of tungsta on these catalysts. Furthermore, for the first time, a quantitative correlation of these effects with measurements proportional to the concentration of adlineation sites has been demonstrated. It appears that the high activity of the tungsta-promoted catalysts is directly related to small numbers of adlineation sites that result from the decoration of Pt by tungsta suboxides. The loss of Pt sites by decoration is more than compensated by the high NO dissociation activity of these sites.

REFERENCES

1. Regalbuto, J. R., Fleish, T. H., and Wolf, E. E., *J. Catal.* **107,** 114 (1987).
2. Regalbuto, J. R., Allen, C. W., and Wolf, E. E., *J. Catal.*, in press.
3. Boudart, M., Vannice, M. A., and Benson, J. E., *Z. Phys. Chem. Neue Folge* **64,** 171 (1969).
4. Tauster, S. J., *ACS Symp. Ser.* **298,** 1 (1986).
5. Pande, N. K., and Bell, A. T., *Appl. Catal.* **20,** 109 (1986).
6. Pande, N. K., and Bell, A. T., *J. Catal.* **97,** 137 (1986).
7. Gandhi, H. S., Yao, H. C., and Stepien, H. K., *ACS Symp. Ser.* **178,** 143 (1982).
8. Van der Berg, F. G. A., Glezer, J. H. E., and Sachtler, W. M. H., *J. Catal.* **93,** 43 (1985).
9. Rives-Arnau, V., and Munuera, G., *Appl. Surf. Sci.* **6,** 122 (1980).
10. Kaul, D. K., and Wolf, E. E., *J. Catal.* **89,** 348 (1984).
11. Kaul, D. K., and Wolf, E. E., *J. Catal.* **91,** 216 (1985).
12. Regalbuto, J. R., Ph.D. dissertation, Univ. Notre Dame, 1986.
13. Regalbuto, J. R., Kaul, D. K., and Wolf, E. E., *Proc. 8th Int. Congr. Catal.* **3,** 253 (1984).
14. Yates, J. T. Jr., and King, D. A., *Surf. Sci.* **30,** 601 (1972).
15. Arai, H., and Tominaga, H., *J. Catal.* **43,** 131 (1976).
16. Fang, S.-M., and White, J. M., *J. Catal.* **83,** 1 (1983).
17. Klein, R., and Schmidt, L. D., *J. Chem. Phys.* **76,** 3823 (1982).
18. Hicks, R. F., Yen, Q.-J., and Bell, A. T., *J. Catal.* **89,** 498 (1984).
19. Gorte, R. J., and Schmidt, L. D., *Surf. Sci.* **109,** 367 (1981).
20. Lorimer, D., and Bell, A. T., *J. Catal.* **59,** 223 (1979).
21. DeVries, J. E., *et al., J. Catal.* **84,** 8 (1983).
22. Kaul, D. K., Sant, R., and Wolf, E. E., *Chem. Eng. Sci.* **42,** 1399 (1987).
23. Masel, R., *Catal. Rev.-Sci. Eng.* **28,** 335 (1986).
24. Bell, A. T., Levin, M., Rieck, J. S., Salmeron, M., and Somorajai, G. A., Annual AIChE Meeting, Chicago, IL, 1985.
25. Demmin, R. A., Ko, C. S., and Gorte, R. J., *J. Phys. Chem.* **89,** 1151 (1985).